Applied Physics Letters

Carbon dangling-bond center (carbon P_b center) at 4H-SiC(0001)/SiO_2 interface

Cite as: Appl. Phys. Lett. **116**, 071604 (2020); https://doi.org/10.1063/1.5143555
Submitted: 25 December 2019 . Accepted: 07 February 2020 . Published Online: 20 February 2020

T. Umeda, T. Kobayashi, M. Sometani, H. Yano, Y. Matsushita, and S. Harada

Applied Physics Letters ARTICLE scitation.org/journal/apl

Carbon dangling-bond center (carbon P_b center) at 4H-SiC(0001)/SiO_2 interface

Cite as: Appl. Phys. Lett. **116**, 071604 (2020); doi: 10.1063/1.5143555
Submitted: 25 December 2019 · Accepted: 7 February 2020 ·
Published Online: 20 February 2020

T. Umeda,[1,a)] T. Kobayashi,[2] M. Sometani,[3] H. Yano,[1] Y. Matsushita,[2] and S. Harada[3]

AFFILIATIONS

[1]Institute of Applied Physics, University of Tsukuba, Tsukuba 305-8573, Japan
[2]Laboratory for Materials and Structures, Institute of Innovative Research, Tokyo Institute of Technology, Yokohama 226-8503, Japan
[3]National Institute of Advanced Industrial Science and Technology (AIST), Tsukuba 305-8569, Japan

[a)]Author to whom correspondence should be addressed: umeda@bk.tsukuba.ac.jp

ABSTRACT

We identify a carbon dangling-bond center intrinsically formed at thermally oxidized 4H-SiC(0001)/SiO_2 interfaces. Our electrically detected-magnetic-resonance spectroscopy and first-principles calculations demonstrate that this center, which we name "the P_{bC} center," is formed at a carbon adatom on the 4H-SiC(0001) honeycomb-like structure. The P_{bC} center ($Si_3{\equiv}C$-, where "-" represents an unpaired electron) is determined to be a just carbon version of the famous P_b center (Si dangling-bond center, $Si_3{\equiv}Si$-) at Si(111)/SiO_2 interfaces because we found close similarities between their wave functions. The P_{bC} center acts as one of the major interfacial traps in 4H-SiC(0001) metal-oxide-semiconductor field-effect transistors (MOSFETs), which decreases the free-carrier density and the field-effect mobility of 4H-SiC(0001) MOSFETs. The formation of the P_{bC} centers has the role of reducing the oxidation-induced strain, similar to the case of the formation of the P_b centers.

Metal-oxide-semiconductor (MOS) interfaces are crucial for various modern electronic devices.[1] They are the heart of Si MOS field-effect transistors (Si MOSFETs) in state-of-the-art complementary-MOS integrated circuits.[1] The MOS structures are also indispensable to various power devices such as power MOSFETs for power electronics.[2–6] The development of power MOSFETs is expanding over widebandgap semiconductors such as 4H-SiC (bandgap, E_g = 3.26 eV),[2,3] GaN (E_g = 3.4 eV),[4] Ga_2O_3 (E_g = 4.8 eV),[5] and even diamond (E_g =5.4 eV)[6] to meet the demand of continuously growing electric-power consumption. However, the performance of their MOSFETs is generally limited due to the poorer quality of their MOS interfaces, which suffer from many more MOS interface defects than Si-MOS systems.[2–6] In Si, major interface defects are identified as so-called "P_b centers,"[7,8] which are found at every Si(111),[9–11] Si(100),[12,13] and Si(110) surface.[14] Essentially, P_b centers are a family of Si dangling bonds (DBs) intrinsically formed at Si/SiO_2 interfaces.[7,8] Similar to Si-MOS systems, Ge-MOS interfaces also generate the same type of interface defect, i.e., "Ge P_b centers."[15,16] In contrast, wideband-gap semiconductors seem to have no such benchmark model for their MOS interface defects. For instance, 4H-SiC/SiO_2 interfaces have been widely studied over two decades; however, the search for benchmark models of their interface defects is still ongoing.[17–24]

In this Letter, we present a spectroscopic and theoretical identification of a P_b-like interface defect in 4H-SiC MOS systems, which we call the "P_{bC} center." The P_{bC} center is intrinsically formed after thermal oxidation of the 4H-SiC(0001) surface (the Si-face), which is the standard surface of 4H-SiC wafers. This center is just a carbon version of the famous P_b center, i.e., an ideal carbon DB at the interface. We believe that the P_{bC} center is identical to a previous "interface carbon defect" with a typical density of 3–4 × 10^{12} cm^{-2} observed by electron-spin-resonance (ESR) spectroscopy on thermally oxidized 4H-SiC(0001)/SiO_2 substrates.[17,18] Instead of ESR, we here used electrically detected-magnetic-resonance (EDMR) spectroscopy,[19–23] which enabled us to complete a full analysis of ^{13}C and ^{29}Si hyperfine (HF) interactions of this center. Like the P_b center in Si/SiO_2 systems, the formation of the P_{bC} center is closely correlated with relaxation of the oxidation-induced strain at 4H-SiC/SiO_2 interfaces, which was quantitatively confirmed from first-principles calculations. The calculations also demonstrated that the P_{bC} center is formed at a carbon adatom (C adatom) on the 4H-SiC(0001) surface. We also discuss significant influences of the P_{bC} center on the performance of 4H-SiC MOSFETs.

For highly sensitive EDMR measurements, we prepared *n*-channel lateral 4H-SiC MOSFETs with a special dimension (gate length/

width = 5/2000 μm) on a 4°-off p-type 4H-SiC(0001) epitaxial layer (Al doping of 5×10^{15} cm^{-3}). The 30-nm thick gate oxide was formed by a standard thermal oxidation at 1200 °C using dry O_2. Further details of the fabrication processes are published in previous papers.[25] The MOSFETs exhibited a maximum field-effect mobility (μ_{FE}) of 7 cm^2 V^{-1} s^{-1}, which is slightly higher than conventional values of Si-face 4H-SiC MOSFETs,[2,3,25] because of optimal dry oxidation and epitaxial layer. However, this value is still far from an ideal electron mobility of 4H-SiC (1000 cm^2 V^{-1} s^{-1}[2,3]), indicating a great influence of interface defects. We then conducted bipolar-amplification-effect (BAE) EDMR measurements[19] to amplify EDMR signals of the interface defects. We used a standard lock-in amplification technique synchronized to a magnetic-field modulation at 1.56 kHz.[18,23] ESR transitions were excited by a microwave at 9.45 GHz and 200 mW at room temperature.

Figure 1(a) shows room-temperature EDMR spectra of the Si-face 4H-SiC MOSFET as a function of magnetic-field angles. Only one strong EDMR signal was observed, which is the P_{bC}-center signal (an electron spin = 1/2), showing slightly c-axial gyromagnetic factors (g) of $g_{//} = 2.0029$ and $g_{\perp} = 2.0032$. We believe that this EDMR signal is identical to an ESR signal with a spin density of $3–4 \times 10^{12}$ cm^{-2} observed in the as-oxidized 4H-SiC(0001) epitaxial layers.[17,18] An extremely higher signal-to-noise ratio of EDMR spectra can reveal a full angular dependence of HF interactions of this center.

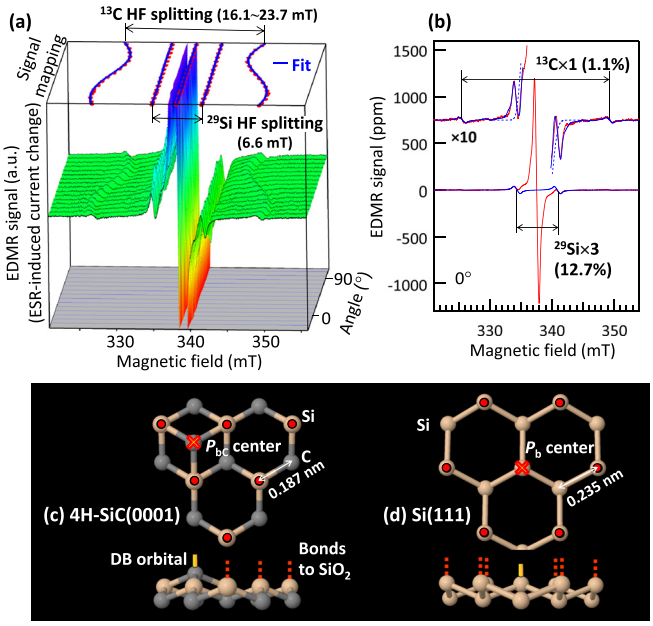

FIG. 1. (a) EDMR spectroscopy on the P_{bC} center at the 4H-SiC(0001)/SiO$_2$ interface as a function of magnetic-field angles. For 0° and 90°, the magnetic field was parallel and perpendicular to the [0001] axis, respectively. Solid blue lines in the angular map (upper plane of this graph) were simulated using the g and HF tensors shown in the text. EDMR spectra were measured using a source current of 180 nA with a negative gate bias of −7.5 V and a constant drain current of −10 μA in BAE EDMR mode. (b) Spectral simulation of ^{13}C and ^{29}Si HF doublet signals (solid blue lines). The ^{29}Si HF structure was fitted to the experimental spectrum by adding smooth tail curves (dashed blue lines in the upper spectrum). Each HF signal consists of replica made from the experimental spectrum with relative intensities shown in figure. (c) Atomic structures of the P_{bC} center at the 4H-SiC(0001) surface and (d) P_b center at the Si(111) surface. In top views, solid circles on Si atoms indicate surface-normal Si bonds. These structures were unrelaxed, and their optimized structures are seen in Fig. 2.

As shown in Fig. 1(a), this center clearly exhibits two sets of HF doublet structures (splitting widths of 16.1–23.7 mT and 6.6 mT), which we assign to HF satellite signals due to a ^{13}C nuclear spin (nuclear spin $I = 1/2$, natural abundance $p = 1.1\%$) and ^{29}Si nuclear spins ($I = 1/2$, $p = 4.7\%$), respectively. These HF signals can be excellently fitted by HF interactions due to one C site and three equivalent Si sites, as demonstrated in Fig. 1(b). The former C site generates HF doublet signals with a relative intensity of 1.1% as shown in the figure. The latter Si sites cause a doublet splitting with a relative intensity of $6[(p/2)^3 + (p/2)(1-p)^2] = 12.7\%$, supposing one to three ^{29}Si nuclear spins at three equivalent Si sites. The ^{13}C HF splitting reveals a c-axial (C_{3v}) symmetry, as seen in the angular map of Fig. 1(a), indicating that the C site has a c-axial 2p-orbital. The c-axial ^{13}C HF tensor was determined to have $A_{//} = 23.70$ mT and $A_{\perp} = 16.09$ mT.

The above ^{13}C and ^{29}Si HF interactions are in good agreement with a carbon-DB model such as a $Si_3{\equiv}C$- structure ("-" means a DB) at the 4H-SiC(0001)/SiO$_2$ interface, which is just analogous to the P_b center (a $Si_3{\equiv}Si$- structure) at the Si(111)/SiO$_2$ interface.[7,10,11] The largest HF splitting of ^{13}C with a c-axial symmetry is generated from a surface-normal (c-axial) carbon DB. The second largest HF interaction due to ^{29}Si is caused by three equivalent Si atoms adjacent to the C DB site. In Fig. 1(c), we draw the atomic structure of the P_{bC} center at the 4H-SiC(0001) surface, in addition to that of the P_b center at the Si(111) surface [Fig. 1(d)]. Obviously, both surfaces have similar honeycomb-like structures, except their lattice constants. They commonly have surface-normal Si bonds, as indicated by "•" in the figure. The P_b center is formed by breaking one of such Si bonds, as denoted with "×" in Fig. 1(d). In contrast, at the 4H-SiC(0001) surface, there are *no* surface-normal C bonds. Thus, we must consider an additional atomic configuration where a carbon DB stands up. Our conclusion is shown in Fig. 1(c) on the basis of the first-principles calculations. A carbon DB can be formed at a C adatom bonded to three Si atoms on the 4H-SiC(0001) surface. The advantages of such a configuration are obvious, though quantitative arguments will be given later. When connecting to a top SiO$_2$ layer, the Si(111) surface shown in Fig. 1(d) must be affected by a tensile strain due to a larger unit cell of SiO$_2$.[7,8,11,26] Eventually, some Si bonds must be disconnected, resulting in the formation of the P_b center.[7,8,11] On the other hand, since a unit cell of 4H-SiC(0001) is smaller than that of Si(111), we must disconnect more Si bonds at the 4H-SiC(0001)/SiO$_2$ interface. A C-adatom structure consumes three Si bonds at the interface, reducing the above constraint. Simultaneously, it can also fix residual C atoms that are unavoidably emitted during the thermal oxidation of 4H-SiC. Further discussions are shown in Ref. 27.

From the obtained ^{13}C HF tensor, we can experimentally determine the wave function[7,10,13,28,29] of the P_{bC} center, as summarized in Table I. One of the notable features is a very strong spin localization on a DB site for the P_{bC} center. η^2 reaches 80%, which is the largest value obtained in SiC.[29] Such strongest spin localization is also characteristic of the original P_b center in Si.[7,10] Table I also shows the s/p hybridization ratio (α^2/β^2), which is significantly higher for P_{bC} (21%) than for P_b (13%). This indicates a more sp^3-like tetrahedral structure for P_{bC}, which is naturally understandable by the C-adatom structure.

TABLE I. Wave-function parameters of P_{bC} and P_b centers. Fractions of *s*- and *p*-orbitals, $\eta^2\alpha^2$ and $\eta^2\beta^2$ ($\alpha^2 + \beta^2 = 1$), are directly calculated from isotropic and anisotropic HF constants A_{iso} and A_{aniso}, via $\eta^2\alpha^2 = |A_{iso}/A_0|$ and $\eta^2\beta^2 = |b/b_0|$, respectively.[7,10,11,24,28,29] Note that $A_{iso} = (A_{//} + 2A_{\perp})/3$ and $A_{aniso} = (A_{//} - A_{\perp})/3$.[28,29] We used known HF constants of $A_0 = 134.77$ mT and $b_0 = 3.83$ mT for ^{13}C and $A_0 = -163.93$ mT and $b_0 = -4.075$ mT for ^{29}Si.[28] The calculated ^{13}C HF constants of a C adatom were $A_{//} = 10.9$ mT and $A_{\perp} = 4.0$ mT. In lower part, we estimated $\eta^2\alpha^2$ and $\eta^2\beta^2$ in the same manner from the calculated ^{13}C and ^{29}Si HF tensors for P_{bC} and P_b, respectively.

Center	*s*-orbital ($\eta^2\alpha^2$)	*p*-orbital ($\eta^2\beta^2$)	Spin localization (η^2)	*s*/*p* ratio (α^2/β^2)	References
Experiment					
P_{bC} at 4H-SiC(0001)/SiO_2	14%	66%	80%	21%	This work
P_b at Si(111)/SiO_2	7%	53%	60%	13%	10
porous-P_{bC} at *porous*-SiC/SiO_2	4%	35%	39%	11%	24
Theory					
C adatom (P_{bC}) at 4H-SiC(0001)	5%	60%	65%	8%	This work
Si DB (P_b) at Si(111)	6%	60%	66%	9%	This work

In contrast, the original P_b center bound on the Si(111) surface is stabilized into an sp^2-like planar structure.[7,8]

As tabulated in Table I, in *porous*-SiC/SiO_2 structures, different P_{bC} centers (we here call "*porous*-P_{bC}") were observed,[24] showing a quite different nature, e.g., their η^2 is only 39% and their α^2/β^2 (11%) is close to that of P_b. Since such η^2 is widely seen for bulk defects in SiC,[29] the *porous*-P_{bC} centers may be formed in the bulk side of the interfaces. Note that for other previous interface defects such as the "Si-vacancy center"[20,21] and "dual-P_{bC} centers,"[22] complete analyses on their HF interactions and their wave functions have not yet been reported.

To examine the P_{bC} center more quantitatively, we carried out first-principles calculations on both the P_{bC} and P_b centers. All calculations were carried out on the basis of density functional theory by using the Vienna *ab initio* simulation package (VASP). The projector augmented-wave method, as implemented in the VASP code, was applied in the calculations. Figures 2(a) and 2(b) show our H-terminated 4H-SiC(0001) and Si(111) slab units for optimizing the calculations on semiconductor surfaces. They include either a P_{bC} center (a DB on a C adatom) or a P_b center (a Si DB formed at the surface). The lattice parameters of SiC were fixed to the values obtained in our previous calculations,[30,31] and the defect structures were relaxed using the Perdew–Burke–Ernzerhof functional[32] until the remaining forces were less than 40 meV/Å. Note that, by calculating the formation energies of 114 types of mono- and di-carbon defects in 4H-SiC(0001)/SiO_2 systems, we found that the C adatom shown in Fig. 2(a) appears as one of the metastable forms of carbon-related defects.[30,31]

Next, we check the HF constants of the P_{bC} center, which was performed using the Heyd–Scuseria–Ernzerhof (HSE06) hybrid functional.[34–36] The contribution of core states (A_{1c})[36] is included in the calculation of HF constants. A single *k*-point (the Γ point) was sampled during the calculations, and spin-polarization was taken into account. As summarized in Table I, the experimental and theoretical values are basically in good agreement with each other for both the P_{bC} and P_b centers, ensuring the validity of the C-adatom model as well as the validity of our calculation strategy. Only an exception was a smaller calculated value for the 2*s*-orbital ($\eta^2\alpha^2$) of the P_{bC} center. This larger deviation may be related to the fact that the isotropic ^{13}C HF constant is extremely sensitive to the amplitude of the 2*s*-orbital, which is more difficult to be calculated accurately compared to other orbitals.

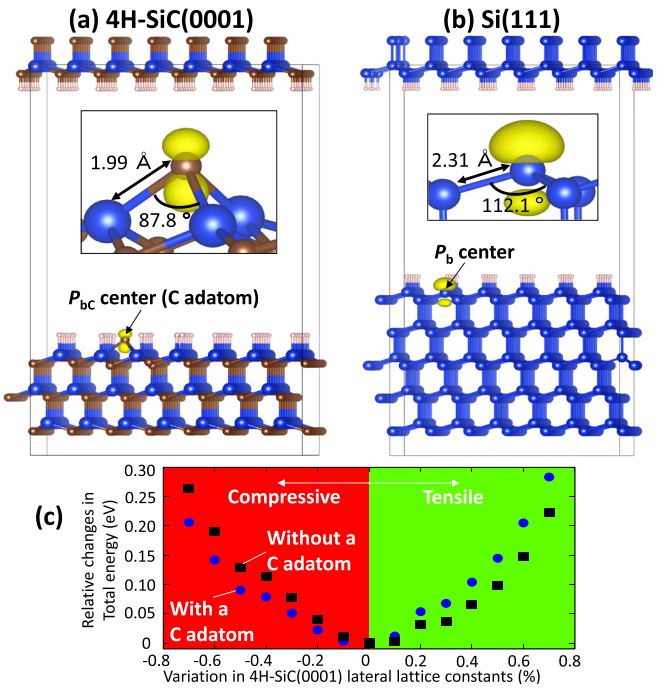

FIG. 2. (a) 488-atom H-terminated 4H-SiC(0001) unit cell including a single P_{bC} center used for first-principles calculations. (b) 503-atom H-terminated Si(111) unit cell for calculating the P_b center. In (a) and (b), blue, brown, and small white balls depict the Si, C, and H atoms, respectively. The vacuum thickness is about 18 Å for each structure. The Si(111) cell was constructed on the algorithm proposed in Ref. 33. The calculated three-dimensional wave functions related to DB states of the C adatom and surface Si atom are also drawn with the isosurface of about 30-% of maximum amplitude. The visualization of crystal structures and wave functions was performed using VESTA. (c) Total-energy calculations on 4H-SiC(0001) unit cells with/without a P_{bC} center under either lateral lattice expansion or compression. The vertical axis indicates relative changes in the calculated total energy, and the horizontal axis denotes relative changes in the lateral lattice constant of unit cells. Zero of lattice constant was set at the optimized lattice constant of the H-terminated 4H-SiC slab.

In Fig. 2(c), we examine the effect of a top SiO_2 layer on the 4H-SiC(0001) surface through the intentional introduction of an in-plane strain into the 4H-SiC unit cell. Here, we optimized the internal atomic positions by the HSE06 functional with the varying in-plane lattice constants. The horizontal axis indicates the introduction of either a tensile strain or compressive strain along two lateral directions. In the C-adatom structure shown in Fig. 2(a), the bond length between the C adatom and three Si atoms is expanded by 6% (1.99 Å) compared to the normal C–Si length (1.88 Å). Therefore, the C-adatom structure should become more stable when it is compressed along the lateral directions. In fact, the energy gain of creating a C-adatom increases under compressive strain, as shown in Figure 2(c). Namely, the C-adatom structure has a tendency to shrink; in other words, it intrinsically involves a local compressive strain. Accordingly, the formation of the C adatoms (the P_{bC} centers) can locally cancel out the oxidation-induced tensile strain.[26] We emphasize that such a strain-induced formation mechanism is just similar to that proposed for the P_b center at the Si(111)/SiO_2 interface.[7,11]

The spin density of the P_b center at the Si(111)/SiO_2 interface was found to be typically $2–3 \times 10^{12}\,cm^{-2}$,[7,9–11] which is approximately 50% smaller than that of the P_{bC} center ($3–4 \times 10^{12}\,cm^{-2}$[17,18]) at the 4H-SiC(0001)/SiO_2 interface. This ratio is similar to that of the atomic densities between the Si(111) and 4H-SiC(0001) surfaces: 7.8×10^{14} and $1.2 \times 10^{15}\,cm^{-2}$ for their top Si atoms, respectively,. In Ref. 18, we demonstrated hydrogen passivation of the P_{bC} center, providing with another similarity to the P_b center.

Since the above spin density is just comparable to the free-carrier density in the inversion layer of 4H-SiC MOSFETs ($< 9 \times 10^{12}\,cm^{-2}$),[25] the P_{bC} center has non-negligible impacts on the performance of the MOSFETs. Actually, we observed that the P_{bC} center was diminished by 1/10 or less after post oxidation anneal (POA) with NO, which simultaneously increased μ_{FE} over $30\,cm^2\,V^{-1}\,s^{-1}$.[18] The physical reasons why the P_{bC} center affects μ_{FE} are because (1) this center reduces the amount of mobile electrons via electron capture and (2) charged P_{bC} centers (charged DBs) increase Coulombic scattering. In fact, an increase of $\sim 2 \times 10^{12}\,cm^{-2}$ was observed in the free-carrier density after NO POA,[25] which is comparable to the density of P_{bC}. However, the P_{bC} center cannot account for the total amount of electron traps ($\leq 8 \times 10^{12}\,cm^{-2}$[25]) and other traps should also be present. The electronic level of P_{bC} will also be important for *p*-channel 4H-SiC MOSFETs, because of its amphoteric nature likewise the P_b center. Its exact location is being examined experimentally and theoretically. At least, we estimate that its neutral DB level (spin-1/2 state) is located in the midgap region because the P_{bC} center became EDMR-active under a negative gate bias [c.f., Fig. 1(a)].

In summary, we established a benchmark model of a typical interface defect in 4H-SiC(0001)/SiO_2 systems. In this most studied wideband-gap-semiconductor MOS interface, the P_{bC} center (carbon DB) is intrinsically formed in association with the oxidation-induced strain. We unambiguously identified that this center is just a carbon version of the famous P_b center in Si-MOS systems, based on the first full-analysis on ^{13}C HF interaction of an interfacial C atom.

This work was supported by the Council for Science, Technology and Innovation (CSTI), Cross-ministerial Strategic Innovation Promotion Program (SIP), "Next-generation power electronics" (funding agency: NEDO). This work was also, partly, supported by Grant-in-Aids (Grant Nos. 18H03770, 18H03873, and 17H02781) from the Ministry of Education, Culture, Sports, Science and Technology of Japan. Computations were performed, mainly, at the Center for Computational Science, University of Tsukuba, and the Supercomputer Center at the Institute for Solid State Physics, The University of Tokyo.

REFERENCES

[1]S. M. Sze and K. K. Ng, *Physics of Semiconductor Devices Third Ed.* (John Wiley & Sons, New York, 2007).
[2]G. Liu, B. R. Tuttle, and S. Dhar, Appl. Phys. Rev. **2**, 021307 (2015).
[3]T. Kimoto and J. A. Cooper, *Fundamentals of Silicon Carbide Technology* (Wiley, Singapore, 2014).
[4]T. Oka, T. Ina, Y. Ueno, and J. Nishii, Appl. Phys. Express **8**, 054101 (2015).
[5]S. J. Pearton, F. Ren, M. Tadjer, and J. Kim, J. Appl. Phys. **124**, 220901 (2018).
[6]T. Matsumoto, H. Kato, K. Oyama, R. Arai, T. Makino, M. Ogura, D. Takeuchi, T. Inokuma, N. Tokuda, and S. Yamasaki, Sci. Rep. **6**, 31585 (2016).
[7]P. M. Lenahan and J. F. Conley, Jr., J. Vac. Sci. Technol., B **16**, 2134 (1998).
[8]A. Stirling, A. Pasquarello, J.-C. Charlier, and R. Car, Phys. Rev. Lett. **85**, 2773 (2000).
[9]Y. Nishi, Jpn. J. Appl. Phys., Part 1 **10**, 52 (1971).
[10]K. L. Brower, Appl. Phys. Lett. **43**, 1111 (1983).
[11]A. Stesmans and B. Nouwen, Phys. Rev. B **61**, 16068 (2000).
[12]A. Stesmans and V. V. Afanas'ev, J. Appl. Phys. **83**, 2449 (1998).
[13]A. Stesmans, B. Nouwen, and V. V. Afanas'ev, Phys. Rev. B **58**, 15801 (1998).
[14]M. Jivănescu, A. Stesmans, R. Kurstjens, and F. Dross, Jpn. J. Appl. Phys., Part 1 **52**, 041301 (2013).
[15]S. Paleari, A. Molle, and M. Fanciulli, Appl. Phys. Lett. **93**, 242105 (2008).
[16]S. Paleari, A. Molle, and M. Fanciulli, Phys. Rev. Lett. **110**, 206101 (2013).
[17]T. Umeda, G.-W. Kim, T. Okuda, M. Sometani, T. Kimoto, and S. Harada, Appl. Phys. Lett. **113**, 061605 (2018).
[18]T. Umeda, Y. Nakano, E. Higa, T. Okuda, T. Kimoto, T. Hosoi, H. Watanabe, M. Sometani, and S. Harada, J. Appl. Phys. (unpublished).
[19]T. Aichinger and P. M. Lenahan, Appl. Phys. Lett. **101**, 083504 (2012).
[20]C. J. Cochrane, P. M. Lenahan, and A. J. Lelis, J. Appl. Phys. **109**, 014506 (2011).
[21]C. J. Cochrane, P. M. Lenahan, and A. J. Lelis, Appl. Phys. Lett. **100**, 023509 (2012).
[22]G. Gruber, J. Cottom, R. Meszaros, M. Koch, G. Pobegen, T. Aichinger, D. Peters, and P. Hadley, J. Appl. Phys. **123**, 161514 (2018).
[23]T. Umeda, Y. Kagoyama, K. Tomita, Y. Abe, M. Sometani, M. Okamoto, S. Harada, and T. Hatakeyama, Appl. Phys. Lett. **115**, 151602 (2019).
[24]J. L. Cantin, H. J. von Bardeleben, Y. Shishkin, Y. Ke, R. P. Devaty, and W. J. Choyke, Phys. Rev. Lett. **92**, 015502 (2004).
[25]T. Hatakeyama, Y. Kiuchi, M. Sometani, S. Harada, D. Okamoto, H. Yano, Y. Yonezawa, and H. Okumura, Appl. Phys. Express **10**, 046601 (2017) and references therein.
[26]X. Li, A. Ermakov, V. Amarasinghe, E. Garfunkel, T. Gustafsson, and L. C. Feldman, Appl. Phys. Lett. **110**, 141604 (2017).
[27]As discussed in Ref. 26, an interfacial strain or a compressive strain in a SiO_2 layer is divided into two components, σ_{th} and σ_{in}, which originate from a thermal expansion mismatch and a structural mismatch, respectively. Quantitative research studies showed that $\sigma_{th} = -0.17$ GPa and $\sigma_{in} = -0.23$ GPa in a Si/SiO_2 system, while $\sigma_{th} = -0.24$ GPa and $\sigma_{in} \approx -0.07$ GPa in a 4H-SiC(0001)/SiO_2 system.[26] Therefore, despite the large structural mismatch between 4H-SiC(0001) and SiO_2, the residual σ_{in} was largely relaxed in SiC. We speculate that the presence of C adatoms contributes to this relaxation.
[28]J. A. Weil, J. R. Bolton, and J. E. Wertz, *Electron Paramagnetic Resonance* (John Wiley & Sons, New York, 1994).
[29]J. Isoya, T. Umeda, N. Mizuochi, N. T. Son, E. Janzén, and T. Ohshima, Phys. Statuss Solidi B **245**, 1298 (2008).

[30]T. Kobayashi, K. Harada, Y. Kumagai, F. Oba, and Y. Matsushita, J. Appl. Phys. **125**, 125701 (2019).
[31]T. Kobayashi and Y. Matsushita, J. Appl. Phys. **126**, 145302 (2019).
[32]J. P. Perdew, K. Burke, and M. Ernzerhof, Phys. Rev. Lett. **77**, 3865 (1996).
[33]Y. Hinuma, Y. Kumagai, F. Oba, and I. Tanaka, Comp. Mater. Sci. **113**, 221 (2016).
[34]H. J. S. Ge and M. Ernzerhof, J. Chem. Phys. **118**, 8207 (2003); **124**, 219906 (2006).
[35]Y. Matsushita, K. Nakamura, and A. Oshiyama, Phys. Rev. B **84**, 075205 (2011) and references therein.
[36]K. Szász, T. Hornos, M. Marsman, and A. Gali, Phys. Rev. B **88**, 075202 (2013).